The Molecular Basis for Antimicrobial Activity of Pore-Forming Cyclic Peptides

Cirac, Anna D.; Moiset, Gemma; Mika, Jacek T.; Kocer, Armagan; Salvador, Pedro; Poolman, Bert; Marrink, Siewert J.; Sengupta, Durba

Published in:
Biophysical Journal

DOI:
10.1016/j.bpj.2011.03.057

Publication date:
2011

The Molecular Basis for Antimicrobial Activity of Pore-Forming Cyclic Peptides

Anna D. Cirac,[†‡] Gemma Moiset,[†] Jacek T. Mika,[†] Armagan Koçer,[†] Pedro Salvador,[‡] Bert Poolman,[†] Siewert J. Marrink,[†*] and Durba Sengupta[†*]

[†]Department of Biochemistry and Biophysical Chemistry, Groningen Biomolecular Sciences, Netherlands Proteomics Centre and Biotechnology Institute and Zernike Institute for Advanced Materials, University of Groningen, Nijenborgh, Groningen, The Netherlands; and [‡]Institute of Computational Chemistry, University of Girona, Girona, Spain

ABSTRACT The mechanism of action of antimicrobial peptides is, to our knowledge, still poorly understood. To probe the biophysical characteristics that confer activity, we present here a molecular-dynamics and biophysical study of a cyclic antimicrobial peptide and its inactive linear analog. In the simulations, the cyclic peptide caused large perturbations in the bilayer and cooperatively opened a disordered toroidal pore, 1–2 nm in diameter. Electrophysiology measurements confirm discrete poration events of comparable size. We also show that lysine residues aligning parallel to each other in the cyclic but not linear peptide are crucial for function. By employing dual-color fluorescence burst analysis, we show that both peptides are able to fuse/aggregate liposomes but only the cyclic peptide is able to porate them. The results provide detailed insight on the molecular basis of activity of cyclic antimicrobial peptides.

INTRODUCTION

How antimicrobial peptides (AMPs) kill bacteria by interacting with the cell membrane is not fully understood. These peptides, often small and cationic, are secreted into the aqueous phase, usually in an unfolded state and bind quickly to the target membrane, where secondary structure may be induced (1–8). At a certain threshold concentration, antimicrobial peptides permeabilize the membrane, either by forming a discrete pore or by disrupting the bilayer structure (2,4,6,9–19). For linear α-helical peptides, the barrel-stave and toroidal-shaped model have been proposed as pore structures (2,3,15,20–23). In addition, a disordered toroidal pore has been proposed for linear antimicrobial peptides from molecular-dynamics (MD) simulations (24–26).

Cyclic AMPs have emerged as good antimicrobial candidates due to their robust secondary structure and high activity (27–29). Gramicidin S, a cationic decapeptide, is one of the best-studied cyclic AMPs (27,28,30–32) and has been shown to permeabilize bilayers but not to stabilize well-defined pores (33). MD simulations have shown that cyclic peptides such as gramicidin S (34,35) and arenicin-2 (36) have β-structures with a relatively rigid backbone conformation. Arginine-rich cyclic peptides have been shown to assemble into nanotubes and extrude the bilayer in MD simulations (37). In general, the molecular details of the action of cyclic AMPs, such as whether these short peptides can open and stabilize pores, as well as the molecular basis for their increased activity, is still unclear.

The focus of our work is a cyclic antimicrobial peptide, BPC194, that was chosen as the best candidate from a library of de novo synthesized cyclic peptides (38,39). The cyclic peptide shows a high antimicrobial activity to different plant pathogenic bacteria (*Erwinia amylovora*, *Pseudomonas syringae*, and *Xanthomonas vesicatoria*). Here, we present a combined MD and biophysical study of the cyclic peptide interacting with anionic lipid bilayers to understand its mechanism of action.

The linear analog BPC193, which is not active, has also been studied, allowing us to reveal the functionally important structural characteristics. We show that only the cyclic peptide is able to form pores in anionic membranes in line with its enhanced antimicrobial activity. The pore size was validated by three independent approaches—MD simulations, electrophysiology, dual-color fluorescence burst analysis (DCFBA), and fluorescence imaging. We further extract the functionally relevant structural properties of the peptides and show the importance of charged residues in forming and stabilizing pores. Finally, an intermediate state was identified which is close to the real transition state during pore formation.

MATERIALS AND METHODS

Molecular dynamics simulations

System setup

MD simulations were performed for systems containing nine peptides, (BPC 194 c(KKLKKFKKLQ), BPC 193 H-KKLKKFKKLQ-OH), and a fully solvated DPPG (dipalmitoyl-phosphatidylglycerol; anionic lipid)

Submitted January 25, 2011, and accepted for publication March 31, 2011.

*Correspondence: d.sengupta@rug.nl or s.j.marrink@rug.nl

Editor: Paulo F. Almeida.

0006-3495/11/05/2422/10 $2.00

doi: 10.1016/j.bpj.2011.03.057

bilayer. The simulations were carried out at a peptide/lipid (P/L) of 9:128 for both cyclic and linear analogs together with 6000~8000 water molecules and 128 K^+ as counterions for anionic lipids. The peptides were initially placed in the water phase at a distance of 1.5–2.3 nm from the membrane surface. The initial structure of the peptides was modeled using the LEAP module of AMBER 9 (40), as unstructured peptides with no intramolecular hydrogen bonds. Multiple simulations were run from different initial random velocity distributions (see Table S1 in the Supporting Material).

Setup for transition state simulations

A snapshot at 109 ns was taken from the simulation 9Ca (Table S1) as an example of the transition state. From this system, 10 simulations were performed with different initial velocity distributions. The transition state was also modified to substitute the cyclic peptide by the linear analog. This substitution was made by cutting the peptide bond between N-terminal residue and the C-terminal residue, as well as adding the corresponding missing atoms. The system was simulated as a linear peptide but with the initial conformation of the cyclic peptide (the so-called hairpin conformation). Further, a harmonic potential was applied to the linear peptide to pull the N-terminal from C-terminal to obtain a random-coil conformation in the transition state. For the modified systems, a minimization was carried out followed by an equilibration with constraints on phosphorus atom and water molecules to keep the position of the transition state. Ten simulations were run for the hairpin conformation and two of the random-coil conformation by changing the starting random velocities of a fully solvated DPPG bilayer.

Analysis

The secondary structure of the peptides was calculated by using the DSSP code (41). For the cyclic peptide, the N-terminal residue K^1 and C-terminal residue Q^{10} that are present in the turn region were neglected while calculating the secondary structure. The structural properties were then calculated from the average number of residues involved in each secondary structural feature along the simulation. The total β-structure is reported as the sum of β-sheet and β-bridge and the total nonstructured as the sum of coil, bend, and turn. The persistence of structure over time was calculated as the percentage of time the β-structure was present.

Simulation parameters

All MD simulations were performed with the GROMACS software package (42). The peptide and peptide-solvent interactions were described by the GROMOS force field 43a2 (43). The force field for DPPG lipids was optimized from DPPC (44) and POPG (45) lipids, compatible with the GROMOS96 parameters. The choline headgroups were replaced by glycerol from the POPG force field, and the tail parameters were taken from the DPPC force field. The parameters were then optimized to achieve an area per lipid consistent with experiment (46).

The equilibrated DPPG bilayer had a thickness of 3.54 $\pm$ 0.05 nm and an area per lipid of 0.69 $\pm$ 0.01 nm^2. The force fields have been parameterized for use with a group-based twin-range cutoff scheme (using cutoffs of 1.0/1.4 nm and a pair-list update frequency of once per 10 steps), including a reaction field (47) correction with a dielectric constant of 78 to account for the truncation of long-range electrostatic interactions. The water was modeled using the SPC (simple-point charge) model (48).

The simulations were performed using periodic boundary conditions and a time step of 2 fs was used. The temperature was weakly coupled (coupling time 0.1 ps) to $T = 320$ K, using the Berendsen thermostat (49). The pressure was weakly coupled (coupling time of 1.0 ps and compressibility of 4.5×10^{-5}), using a semiisotropic coupling scheme in which the lateral ($P_|$) and perpendicular (P_Z) pressures are coupled independently at 1 bar, corresponding to a tension-free state of the membrane. The simulation setup is similar to that used in previous studies of peptide-membrane interactions (25,26,50). For a general review on MD studies of peptide-membrane interactions, see Bond and Khalid (51) and Mátyus et al. (52).

Biophysical characterization

Electrophysiology measurements

A planar lipid bilayer setup was used as described below. The bilayer was formed by painting with 1 μL of a 20 mg/mL solution of 1,2-dioleoyl-*sn*-glycero-3-phosphatidylglycerol lipid (DOPG; Avanti Polar Lipids, Alabaster, AL) in *n*-decane (Sigma-Aldrich, St. Louis, MO) across the 250 μm opening of a Delrin cup that separates two solution-filled compartments, designated *cis* and *trans* (53–55). Both compartments were filled with a buffer solution consisting of 10 mM 2-(4-(2-hydroxyethyl)-1-piperazinyl)-ethanesulfonic acid (HEPES; Roche Diagnostics, Mannheim, Germany), pH 7.0, containing 150 mM NaCl (Merck, Whitehouse Station, NJ), further referred to as buffer A. The transmembrane current (I_m) under different applied potentials (V) was monitored, using an integrating Bilayer Clamp Amplifier BC-535 (Warner Instruments, Harvard Apparatus, Hamden, CT). Currents were filtered through an eight-pole low-pass Bessel filter model No. LPF-8 (Warner Instruments) and digitized using Clampex 10.2 software (Axon Molecular Devices, Union City, CA).

Membrane conductance (G_m) events were identified as $G_m = I_m/V$ and analyzed with the Clampfit software (Axon Molecular Devices) (56). Only membranes with capacitances between 80 and 120 pF were used, which correspond to membrane diameters of 50–61 μm. Before adding the peptide, the membranes were controlled for the lack of any leakage by applying the same range of voltage as in the presence of peptide. The peptides at 3 and 10 μM were added to the *cis* side of the planar lipid bilayer and stirred for 1 min without applying voltage. In some cases a voltage of $\pm$40 mV was applied to preactivate the peptide and decrease the time needed to observe activity. Subsequently, the conductance was recorded at different voltages ranging from 0 to $\pm$50 mV. Ten traces, total, were each recorded with freshly prepared DOPG membranes. The pore diameter was estimated by an extended version of the model proposed by Hille (57,58) given by (59)

$$d = \frac{\rho g}{\pi}\left(\frac{\pi}{2} + \sqrt{\frac{\pi^2}{4} + \frac{4\pi l}{\rho g}}\right), \tag{1}$$

where d is the diameter of the pore, ρ is the resistivity of the buffer, g is the measured conductance, and l is the length of the pore. The unitary pore conductance, g, was estimated from all recordings. The resistivity of the buffer A was assumed to be 80 Ωm (58). The length of the pore equals the membrane thickness and was assumed to be 3.5 nm.

Dual-color fluorescence burst analysis

In the DCFBA experiment, liposomes were labeled with two spectrally nonoverlapping fluorescent probes (60). One probe was incorporated in the phospholipid bilayer, whereas the other filled the aqueous interior of the liposome. By using a dual-color laser-scanning microscope, we monitored membrane-disrupting effects at the single liposome level. The results are presented in the DCFBA profiles as the population-distribution histogram of liposomes with a given internal marker concentration, C_i, given by

$$C_i = \frac{\int_{t1}^{t2} I_{SM}\,dt}{\left(\int_{t1}^{t2} I_L\,dt\right)^{3/2}}, \tag{2}$$

where I_L is the fluorescence of the lipid marker and I_{SM} is the fluorescence of the internal size marker in each fluorescence burst (61).

The average fluorophore population, P_{av}^{fluor}, is given by

$$P_{av}^{fluor} = \frac{\int_{t1}^{t2} \frac{I_{fluor}}{N_{peaks}}\,dt}{\int_{t1}^{t2} \frac{I_{fluor}^0}{N_{peaks}^0}\,dt}, \tag{3}$$

where I_{fluor} is the fluorescence intensity of each peak above a given threshold for every P/L ratio; I^0_{fluor} is I_{fluor} at P/L = 0; N_{peaks} is the number of peaks at every P/L; and N^0_{peaks} is N_{peaks} at P/L = 0. The relative population of the internal size marker, P^{SM}_{rel}, is given by

$$P^{SM}_{rel} = \frac{P^{SM}_{av}}{P^{membr}_{av}}, \quad (4)$$

where P^{SM}_{av} is the average internal marker population and P^{membr}_{av} is the average membrane fluorophore population.

DCFBA assay

Liposomes were prepared as described by van den Bogaart (60). Briefly, 1,1′-dioctadecyl-3,3,3′,3′-tetramethylindodicarbo-cyanine perchlorate (DiD; Invitrogen, Carlsbad, CA) labeled-liposomes were prepared by rehydration of a dried lipid film in the presence of glutathione (GSH)-labeled Alexa Fluor 488 (AF488; Invitrogen) as a aqueous phase marker in buffer A. The DiD/DOPG molar ratio was 1:12,000. Subsequently, the liposomes were extruded 11 times through a 200-nm polycarbonate filter (AVESTIN, Ottawa, Ontario, Canada). The liposomes were separated from the nonencapsulated fluorophores by centrifugation (20 min, 270,000 × *g*, 20°C) and resuspended in buffer A to a final concentration of 5 mg/mL DOPG.

Fluorescence burst analysis was carried out on a laser-scanning confocal microscope (62), as described by van den Bogaart (17,60,63). Different amounts of peptide were added to 64 μg/mL DOPG liposomal solutions, yielding final peptide/lipid ratios from 1:52 to 5:1. The samples were equilibrated for 10 min at room temperature after each addition of peptide. The fluorescence bursts were measured for 10 min. To estimate the size of the pore, a size marker was encapsulated inside the DiD-labeled vesicles, i.e., 10 kDa dextran labeled with fluorescein (Invitrogen).

RESULTS AND DISCUSSION

The cyclic peptide causes large perturbations in DPPG bilayers

Simulations were performed with BPC194 interacting with a DPPG bilayer at a P/L of 9:128. Phosphatidylglycerol bilayers were chosen because the peptide is antimicrobial (characterized by anionic lipids) with low hemolytic activity (characterized by zwitterionic lipids). Previous results indicated that BPC194 was the most active in 100% PG membranes (64). The time course of a particular simulation (see Table S1, 9Ca) is depicted in Fig. 1 *A*, but similar behavior was observed in the remaining simulations (see Table S1, 9Cb–9Cg). The peptides were initially placed in the water layer close to the bilayer (0 ns) and subsequently

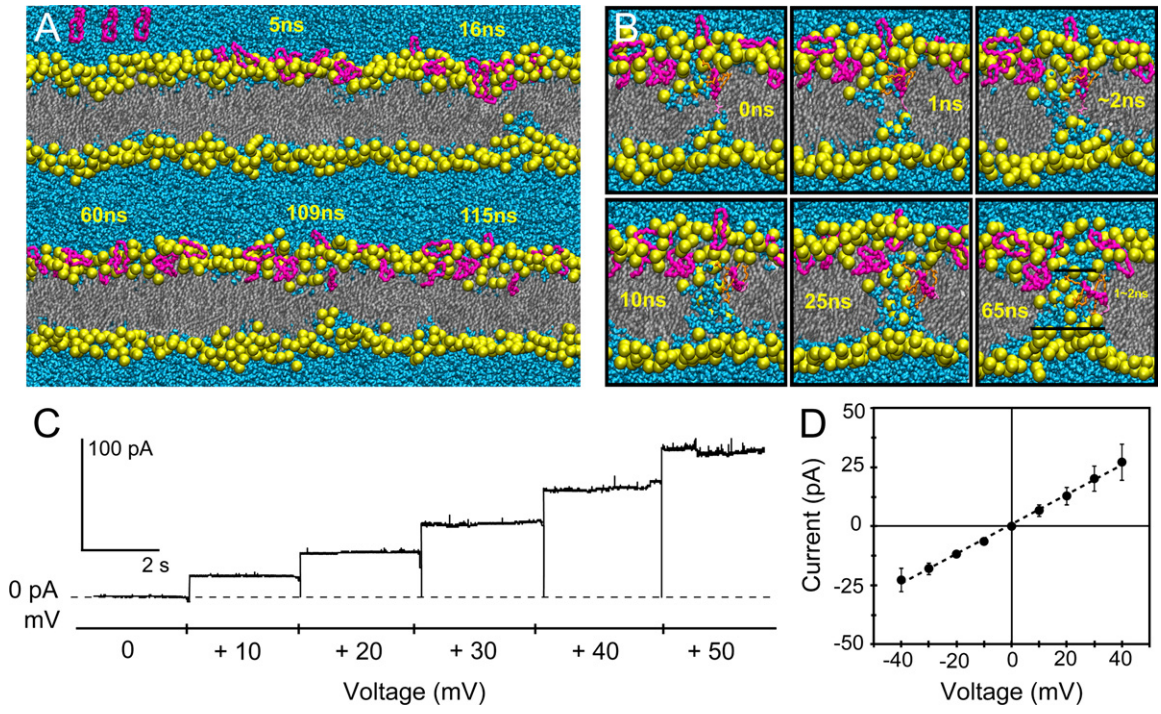

FIGURE 1 The cyclic peptides cause large fluctuations in the membrane upon binding and can form a disordered toroidal pore. (*A*) Time course of the simulation 9Ca. At 0 ns, all peptides were placed close to the bilayer and they bound within 5 ns. The first perturbation of the inner leaflet was seen at 16 ns, when some lipids were pulled into the bilayer due to the action of the cyclic peptide. The highest perturbation was at 109 ns and involved three peptides, one of which adopts a transmembrane orientation. The inner leaflet relaxed at 115 ns. (*B*) The snapshot of the transition state (*A*, 109 ns) was taken as the starting structure (0 ns). An increase of the number of water molecules inserting into the bilayer was followed by the opening of a water channel (1–2 ns) and insertion of lipid headgroups further inside to form a toroidal-shaped pore (10–25 ns). A stable toroidal-shaped pore was seen at 65 ns. The lipid headgroups are depicted in large spheres. The peptide backbone is shown as thick sticks, lipid tails as thin sticks, and water molecules as small spheres. In the online figure, the cyclic peptide, BPC194, is always depicted in pink. To clarify the bridging of the two leaflets in the transition state, the lysine residues and the glutamine residue are shown only for the peptide in a transmembrane orientation. (*C*) Current traces recorded after the addition of BPC194 peptide to DOPG membranes. (*D*) I/V curves plotted from seven independent current trace recordings of BPC194.

bound fast (~5 ns) to the membrane interface. During the simulation, most of the peptides remained bound at the interface, although a few peptides were able to cooperatively perturb the outer leaflet and consequently insert deeper (Fig. 1 *A*, 16–60 ns).

In the perturbed state, the positively-charged residues of the peptides interacted with the closest headgroup moieties and pulled them, together with some water molecules, into the core of the membrane. The peptide-free inner leaflet was also affected by the action of the cyclic peptide bound on the outer leaflet. This behavior was seen repetitively during the simulation and was usually followed by a relaxation of both leaflets. Occasionally, a much larger perturbation occurred (109 ns), characterized by a decrease in the local lipid-chain order (see Fig. S1 *A*). At this point, the perturbation was caused by a cooperative effect of three peptides, one of which adopted a transmembrane-orientation with its glutamine residue close to the center of the hydrophobic core. In this position, the glutamine residue interacted with some headgroup atoms of the inner leaflet. During this perturbation, a few water molecules were able to cross the membrane. However, the inner leaflet relaxed again and the orientation of the glutamine residue reverted back to the interface (Fig. 1 *A*, 115 ns). Only smaller perturbations of the membrane were observed in the remainder of the simulation.

The cyclic peptide can form a disordered toroidal pore

In our previous simulations of AMP action (25,26), the first event during pore formation was the bridging of the two leaflets by a peptide. Although such an orientation of the peptides was seen in simulation 9Ca (Fig. 1 *A*, 109 ns), it did not lead to a porated state. Nevertheless, we expect this highly perturbed state to be an intermediate, mimicking the transition state toward pore formation. To sample the conformational space around this so-called transition state, 10 simulations were set up. The velocities in the system were varied to provide a different direction on the potential energy surface that may lead to pore formation. Indeed, a pore was formed in six out of ten simulations (for details, see Table S2, C1–C10). The mechanism of the pore formation is depicted in Fig. 1 *B*, using C9 as a representative of all simulations. The first time point (0 ns) was taken as the transition state from which the simulation was started (compare to Fig. 1 *A*, 109 ns).

Water molecules readily inserted into the bilayer and finally after 1~2 ns, some water molecules crossed the bilayer to open a water channel. Headgroup atoms of both leaflets moved inside the membrane core to line the water channel. From then on, the pore remained open and the lipid headgroups of both leaflets rearranged to form a disordered toroidal-shaped pore at ~25 ns. The size of the water channel fluctuated in time as well as along the direction of the pore axis, ranging between ~1 and 2 nm (see Fig. 1 *B*, 65 ns and Fig. S1, *B* and *C*). The pores formed in our simulations could be characterized as disordered toroidal pores with the peptides residing in different positions and orientations. In all cases, the pore was stabilized by three peptides—a dimer and a monomer—with the remaining peptides lying close to the pore. No peptide translocation was seen in the nanosecond time regime of the simulations.

Electrophysiology revealed that pore formation is specific for cyclic peptides

To monitor the pore formation of BPC194, ion fluxes in a planar lipid bilayer setup were measured. An example of a current trace recorded upon addition of BPC194 to the *cis* compartment of the planar lipid bilayer setup is shown in Fig. 1 *C*. A voltage-dependent conductance was observed implying that a pore or channel was formed/opened. These conductance events were stable during the course of the recording, pointing toward the formation of discrete pores. The average I/V curve of all independent recordings is plotted in Fig. 1 *D*.

Because the I/V curve is symmetric, the pores formed by BPC194 are not ion-selective. All independent recordings showed similar unitary pore conductance with an average value of 0.61 $\pm$ 0.12 nS. The diameter of the pore was estimated (see Eq. 1) to range between 1.5 and 1.9 nm. At higher peptide concentrations, we also observed higher overall conductance that was a multiple of the unitary conductance, reflecting the higher probability of pore formation. The same increase in probability of pore formation was observed on applying voltages higher than $\pm$50 mV. However, these extra poration events were transient with shorter dwell times.

The linear peptide does not perturb or porate DPPG bilayers substantially

Simulations of the linear analog interacting with DPPG bilayers were performed under conditions identical to the cyclic peptide (see Table S1, 9La–9Lf). A typical time course of the simulation is depicted in Fig. 2 *A*. Upon binding, the linear peptides somewhat perturb the membrane, albeit much less than the cyclic ones. Larger perturbations leading to a transition state were not seen in any of the simulations with the linear peptide. Although the average thickness of the bilayer is similar for the two peptides (3.7 $\pm$ 0.1 nm for the linear and 3.6 $\pm$ 0.1 nm for the cyclic peptide), the perturbations in the outer leaflet are substantially higher when the cyclic peptide is attached. The fluctuations in the outer leaflet, calculated as the deviation of the phosphorus atoms of the headgroups from their center of mass, are $\pm$0.44 nm for the cyclic peptide in comparison to $\pm$0.29 nm for the linear peptide. These results were supported by the electrophysiology measurements, in which the

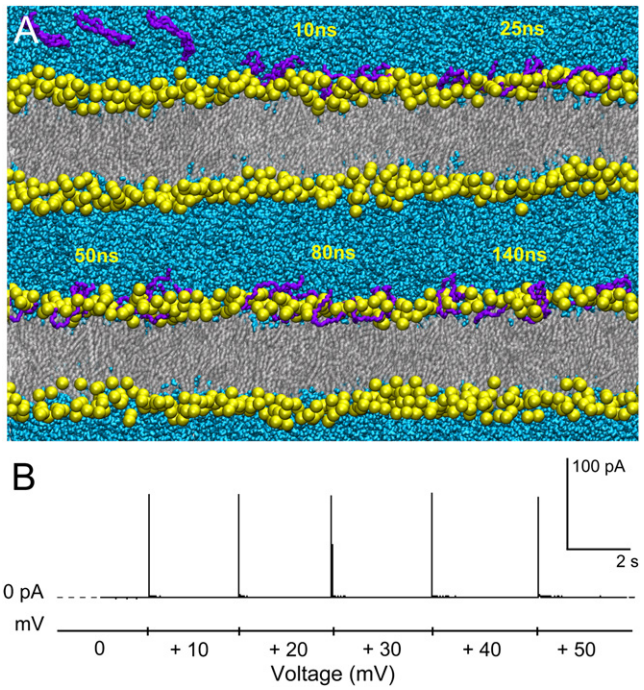

FIGURE 2 The linear peptides do not induce fluctuations in the membrane. (*A*) Time course of the simulation L9a. Initially (0 ns), all linear peptides were placed close to the outer leaflet. Within 10 ns, all peptides bound and remained at the membrane interface. No large perturbations were seen along the simulation (25–140 ns). The headgroups of DPPG are depicted as large spheres, the peptide backbone as thick sticks, and lipid tails as thin sticks. In the online figure, the linear peptide, BPC193, is depicted in purple (*B*) Current traces recorded after the addition of BPC193 peptide to DOPG membranes.

linear analog did not show pore formation or ion flux through the membrane at the same voltage regime in which the cyclic peptide formed pores (Fig. 2 *B*).

Structure-function relationship of the cyclic peptide

To investigate the relation between secondary structure and the ability of the peptides to stabilize a pore, we clustered the peptides depending on how far they lie from the pore and the role they play in stabilizing it (Fig. 3, *A* and *B*). Three classes of peptides were distinguished: those within the rim of the pore (distance 0.3 nm from the center of the pore, region 1), those lying at the mouth of the pore (within 0.3–1.5 nm, region 2), and those not involved in the pore (further away than 1.5 nm, region 3) (Table 1). Peptides in region 1 adopt a stable secondary structure (40% β-structure) in all simulations where a pore is formed (six simulations).

Although the number of residues involved in secondary structure varied among the three peptides, all three showed the longest persistence of β-structure over time (97%). The peptides belonging to region 2 also exhibited a high β-structure (39% for peptides of this region), but the percentage

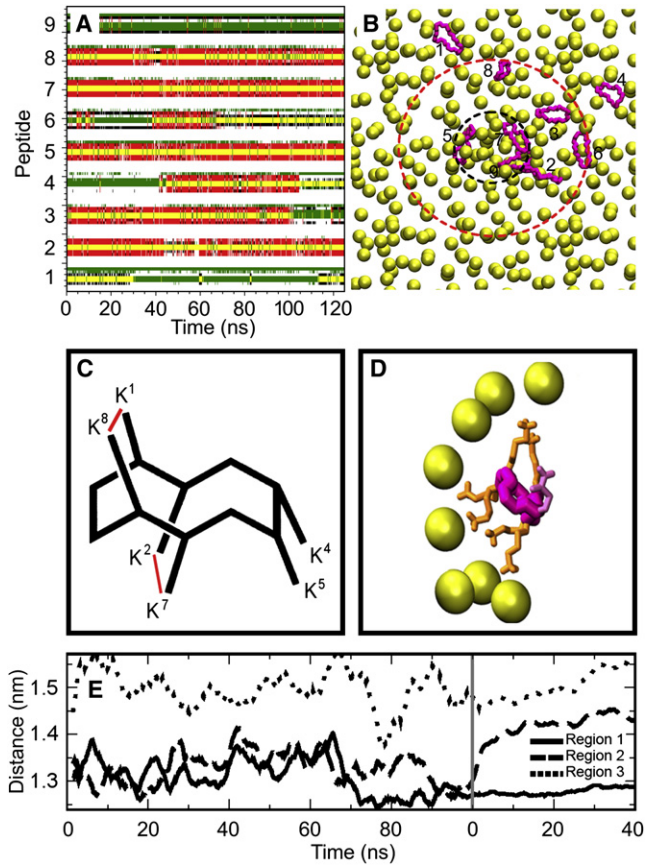

FIGURE 3 Secondary structure related to the distance at the rim of the pore and its function. (*A*) DSSP plot of the secondary structure of all peptides for simulation C9, taking the transition state as the 0-ns time point. (*B*) Top view of the pore showing the positions of the nine peptides. Region 1 peptides are those involved in the pore (within the inner concentric circle). The peptides that remain at the rim of the pore (region 2) are delimited by the outer concentric circle. The peptides furthest from the pore (region 3) are outside the circles. The peptides that remain at the rim of the pore (region 2) are delimited by the red dashed line. The peptides furthest from the pore (region 3) are outside the circles. (*C*) Parallel arrangement of lysine residues in the β-structure (*D*) An example of the aligned lysine residues stabilizing the lipid curvature in the porated state (*side-view* of the pore). (*E*) The average distance between lysine residues K^1-K^8 and K^2- K^7 (plotted as a sum) for peptides in regions 1, 2, and 3. The timescale to the left of the gray line refers to simulation 9Ca (before transition state formation 0–109 ns). The time frame to the right is an average for all simulations (C1–C10) where a pore was formed with the starting time 0-ns being the putative transition state.

fluctuated over time and the persistence of β-structure was 89%. Finally, the peptides in region 3 exhibited multiple folds and adopted different conformations showing only 18% β-structure for the individual peptides.

The apparent importance of the β-structure for stabilization of the pore can be rationalized by considering the relative orientation of the lysine residues. As illustrated in Fig. 3 *C*, the β-structure gives rise to a parallel arrangement of the lysine pairs (K^1-K^8 and K^2-K^7) on the two strands that, presumably, facilitates the interaction of the lysines with the lipid headgroups in the curved geometry of the pore

TABLE 1 Secondary structure and distance from the center of the pore for the peptides belonging to the three regions

Region	Peptide	Distance (nm)	% Coil	% β-structure	% Bend	% Turn	% Time of β-structure
1	5	0.09 ± 0	20.7	45.7	10.3	23.4	94.8
	7	0.09 ± 0	19.6	47.9	8.4	24.1	98.4
	9	0.09 ± 0	25.2	26.2	45.4	3.4	97.7
	Average	0.09 ± 0	22 ± 1	40 ± 6	31 ± 11	17 ± 6	97 ± 1
2	2	0.30 ± 0.05	29.9	43.8	2.8	23.6	92
	3	0.78 ± 0.15	24.8	42.8	12.0	20.4	92.6
	6	1.10 ± 0.15	36.0	32.2	14.2	16.5	91.7
	8	1.50 ± 0.23	30.0	39.1	10.9	20.0	78.1
	Average	0.9 ± 0.2	30 ± 2	39 ± 2	10 ± 2	20 ± 1	89 ± 3
3	4	1.59 ± 0.30	38.5	28.1	15.3	18.2	62.5
	1	2.07 ± 0.25	45.4	8.6	30.9	15.1	33.6
	Average	1.8 ± 0.2	42 ± 2	18 ± 7	23 ± 6	17 ± 1	48 ± 10

The values reported are an average calculated from all simulations where a pore was formed. The center of the pore is defined as the center of mass of the three region 1 peptides that form the pore (backbone only). The time of persistence of β-structure (see Materials and Methods) is also reported. The standard errors reported are calculated from the standard deviation, between all peptides in all simulations.

(Fig. 3 *D*). The distances between the lysine pairs K^1-K^8 and K^2-K^7 (plotted as a sum of the two values) for the three regions of the peptides is shown in Fig. 3 *E*. When the peptides are bound to the membrane (0–109 ns, until *gray line*), the value fluctuates for all three clusters of peptides. However, once the transition state is reached and later when a pore is opened (beyond *gray line*), the distance between the lysine pairs in the peptides in region 1 remained low, consistent with their high persistence of secondary structure. The value for the peptides in region 2 was also low at the transition state but increases as the pore relaxes. The peptides in region 3, which were not involved in the pore, showed the largest distance between the lysine pairs along the simulations.

Transition state alchemy: why the linear peptide cannot stabilize pores

To test whether the β-strand conformation is indeed linked to activity, we repeated the simulations from the transition state with the linear peptide by in silico alchemy, i.e., removing the peptide bond between the first and last residue. The results of these simulations are summarized in Table S2 (L1–L10). In seven of the ten simulations, the bilayer relaxed and the linear peptide moved back to the interface. In the remaining three simulations, a water channel eventually opened. The time course of one of the poration events (L7) is depicted in Fig. 4. Although we observed that the linear peptide is also able to stabilize a water pore (starting from the perturbations caused by the cyclic peptide), the pore differs from the pore formed in the presence of the cyclic peptides:

1. Only one of the three peptides involved in the transition state remained embedded near the central pore region; and
2. The lipid headgroups did not line the pore as clearly as in the case of the cyclic peptide. In most of the simulations, the average percentage of β-structure dropped to a value at ~20%, compared to >30% for the cyclic peptide (compare to Table S2, C1–C10).

In the simulations in which a pore was formed, the peptide nearest the pore preserved a somewhat higher percentage of β-structure (~28%). Two additional unbiased transition state simulations of the linear peptide in its native random-coil conformation were performed. We found that, in the extended conformation, the peptide could not stabilize even those headgroups that were already inserted into the membrane, and the bilayer recovered immediately from the large perturbations induced by the cyclic peptide. An overview of the poration features of the cyclic and linear peptide is presented in Table 2.

DCFBA reveals the mechanism of action on liposomes

Fig. 5 shows the result of DCFBA experiments carried out with BPC194 and BPC193 in the presence of DiD-labeled DOPG vesicles filled with the internal marker, GSH-AF488. In such an experiment, poration of liposomes reduces the internal marker concentration and the DCFBA population histogram shifts to lower concentration values.

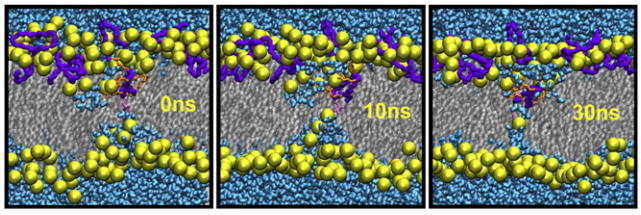

FIGURE 4 The linear peptides cause large perturbations from the in silico modified transition state. Time course of a transient pore formed by a linear peptide (simulation L7). The time point 0-ns corresponds to the transition state taken from the simulation with the cyclic peptide. After 10–30 ns, large perturbations were seen and a few water molecules crossed the bilayer. Please note that in most simulations, the bilayer relaxes and such large perturbations are not seen.

TABLE 2 Summary of pore features created by the cyclic peptide and the linear peptide

Pore features	Cyclic peptide	Linear peptide
Pore propensity	High	Low
Pore diameter	1–2 nm	<1 nm
Number of peptides inside	3	1
% β-structure	34%	21%
Outer leaflet deviation	$\pm$0.55	$\pm$0.48
Number of porated states	6/10	3/10
Number of lipid headgroups	8–11	6–10
Number of water molecules	100–123	76–84
Formation time	1–4 ns	3–30 ns

In contrast, membrane fusion or aggregation results in a decrease in the number of detected liposomes, which is observed as a decrease in the area of the population histogram. For the cyclic analog, at low P/L ratios ($\leq$1), the number of liposomes decreased, which is indicative of fusion or aggregation (Fig. 5 *A*).

The membrane fusion/aggregation activity was confirmed by confocal imaging of the liposomes and was accompanied by leakage of the internal marker (Fig. 5 *A* and *B*, P/L of 0.3). Intriguingly, by adding an excess of peptide (P/L of 1–5) such that the vesicles are completely shielded by peptide preventing aggregation/fusion, the number of detected liposomes was restored and the concentration of molecules inside the liposomes dropped (Fig. 5 *A*, panel γ), which is indicative of pore formation. The linear peptide, BPC193, also caused membrane fusion or aggregation but at higher P/L than its cyclic counterpart (Fig. 5 *B*). This was confirmed by confocal imaging at the highest concentration of the linear peptide (P/L of 5) where large membrane aggregates were formed without loss of the

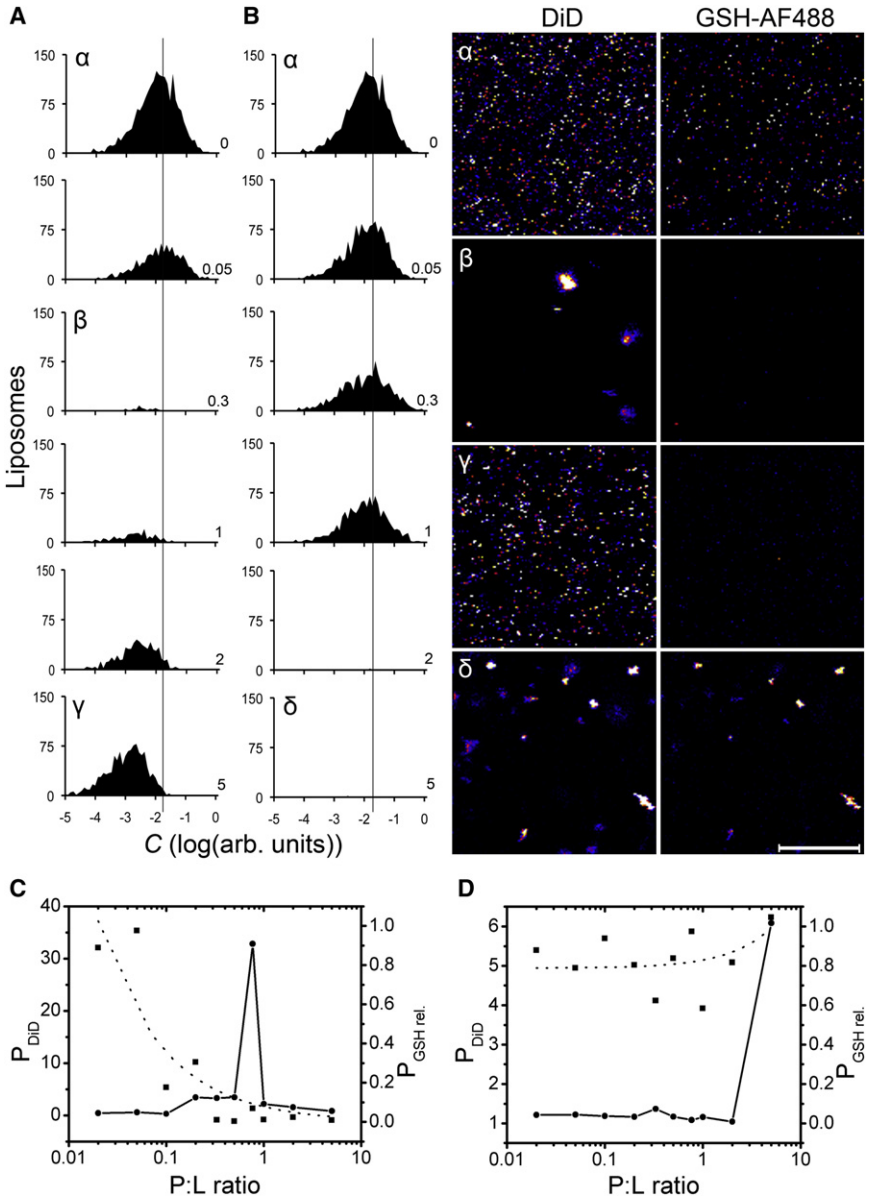

FIGURE 5 Mechanism of action of peptides studied by DCFBA. (*A* and *B*) DCFBA population histograms of BPC194 and BPC193, respectively. Numbers in the subpanels refer to P/L ratios. The *y* axis corresponds to the number of liposomes, and the *x* axis to the arbitrary marker concentration inside the liposomes. (*Right panels*) Confocal images of vesicles probed in the experiments shown in panels *A* and *B*, indicated by Greek symbols (α-δ). (*Leftmost panels*) Membrane probe, DiD. (*Rightmost panels*) Internal marker probe, GSH-AF488. The scale bar is 20 μm. (*C* and *D*) Average DiD population (*circles*, *solid line*) and relative GSH population (*squares*, *dotted line*) for the cyclic and the linear peptide, respectively.

internal marker, indicative of the lack of pore formation (Fig. 5 *A*, panel *δ*).

To present the overall data comprehensively, the average membrane fluorescence per liposome and the relative concentration of the internal marker are plotted in Fig. 5, *C* and *D* (see Materials and Methods for more details). For BPC194, the average membrane fluorescence peaked at a P/L ratio of 0.5–1, while the relative concentration of the internal marker already dropped to zero at a P/L of 0.3. This behavior confirms the leaky fusion/aggregation action of the cyclic peptide. On the other hand, for BPC193, an increase in the membrane population and constant relative internal marker population was seen, thereby corroborating its nonleaky fusion/aggregation propensity.

By using the DCFBA technique and encapsulating bigger internal markers, we could estimate the size of the pore. The smallest molecule that did not leak out was the 10 kDa dextran-fluorescein (see Fig. S2 *A*) with a dimension of 2.1 nm (shortest axis measured assuming is a prolate ellipsoid), whereas GSH-AF488 leaked out with a diameter of ~1.7 nm (see Fig. S2 *B*, measured by fluorescence correlation spectroscopy). We conclude that the size of the pore is between 1.7 and 2.1 nm.

DISCUSSION

Nature of the transition state

The simulations presented here elucidate the nature of the transition state of the poration process. One may assume that starting from a true transition state, the chance of arriving at either side of the transition state barrier is approximately equal (here the porated membrane versus the intact membrane). Although our statistics are necessarily limited, we observe 6 out of 11 simulations with the cyclic peptide to reach a porated state, starting from the state in which a large perturbation was observed in the original simulation (see Table S2, C1–C10). In the remaining 5 out of 11 simulations, counting also the original trajectory, the system relaxed back to the intact membrane state. This intermediate or transition state is characterized by a single peptide bridging the two leaflets (compare to Fig. 1 *B*, 0 ns). The results are in line with kinetic models that suggest such a state is important in pore formation (65).

Disordered toroidal pore

Using the transition state as seen for many independent trajectories, we were able to show that the deepest-embedded peptides may stabilize a toroidal-shaped pore of 1–2 nm diameter, which is in line with the electrophysiology and pore-sizing DCFBA experiments carried out independently. Only two/three peptides actually lie in the pore while some of the remaining peptides line the mouth of the pore and stabilize the membrane curvature. The structure of the pore is reminiscent of pores seen in previous MD studies (24–26,66) and has been termed the disordered toroidal pore.

Structure-function relationship

In this study, comparisons between a cyclic antimicrobial peptide and its inactive linear analog have highlighted the importance of *β*-structure for its activity, similar to that seen for an antitumor cyclic peptide (67). For BPC194, a constrained secondary structure rather than a high percentage of secondary structure was required to stabilize the pore. The importance of the secondary structure, induced on membrane binding and stabilized in the porated state, appears to be the alignment of the charged residues such that they fit the toroidal shape of the pore (compare to Fig. 3 *D*). This explains why the linear peptide is less active—for entropic reasons a folded structure is less favorable. This entropic penalty is prepaid by the cyclic peptide. Thus, the linear peptide cannot open a pore but may stabilize it, if the starting structure is the transition state structure obtained with the cyclic peptide (see Fig. 4).

Conductance, pore properties, and fusion/aggregation

BPC194 forms stable and nonselective ion pores in planar lipid bilayer experiments, with a unitary conductance of 0.61 ± 0.12 nS, corresponding to a pore diameter of 1.5–1.9 nm. This is in contrast to other cyclic peptides such as gramicidin S that do not form stable pores (68). Stable pores have, however, been seen for linear antimicrobial peptides such as alamethicin, magainins, and defensins (69). Both the cyclic and linear peptides are fusogenic or cause aggregation, as indicated by DCFBA measurements, but only the cyclic peptide caused leakage as well. Similar to melittin (61), BPC194 causes leakage at the same concentration regime at which it fuses or aggregates DOPG membranes. However, further studies in this intriguing fusion/aggregation action are in progress.

CONCLUSIONS

There is now compelling evidence that cyclization of certain sequences of membrane-active peptides enhances their antimicrobial performance. In this article, we analyze the molecular basis for the differences in activity of analogous cyclic and linear antimicrobial peptides. We show that the molecular basis for the enhanced activity resides most likely in the restriction of the number of conformations in the cyclic peptide. We show that it can adopt a favorable orientation toward the membrane and acquire an ordered structure that allows a high charge density and amphipathic arrangement.

The latter allows the cyclic peptide to perturb the membrane substantially and to form discrete pores. Cyclization of the linear sequence locks the peptide in a poration-ready state, allowing it to perturb the bilayer and stabilize the curvature of a toroidal transmembrane pore. Without cyclization, entropy destabilizes the formation of a folded structure and consequently its amphipathic-like character, and hence the linear peptide has a much lower propensity to induce pores. The work presented here provides detailed insight into the mode of action of cyclic peptides and will aid rational design of new antimicrobial molecules.

SUPPORTING MATERIAL

Two figures and two tables are available at http://www.biophysj.org/biophysj/supplemental/S0006-3495(11)00415-2.

The authors thank the Laboratori d'Innovació en Processos i Productes de Síntesi Orgànica group (University of Girona), for help with the synthesis of the peptides.

We acknowledge financial support from the Spanish Ministerio de Ciencia e Innovación (grant No. MAT2008-04834 to A.D.C. and P.S.) and Spanish Ministerio de Ciencia e Innovación (grant No. BES-2006-11671, in the form of a doctoral fellowship to A.D.C.); the Netherlands Organization for Scientific Research;NWO (grant to D.S. and S.J.M.); SysMo via the Biotechnology and Biological Sciences Research Council-funded KosmoBac program (to B.P.); Netherlands Organization for Scientific Research (TOP-subsidy grant No. 700-56-302 to B.P.; Vidi grant to A.K.); European Research Council starting grant (to A.K.); and the Zernike Institute for Advanced Materials to support the appointment and research of G.M. and J.T.M.

REFERENCES

1. Brogden, K. A. 2005. Antimicrobial peptides: pore formers or metabolic inhibitors in bacteria? *Nat. Rev. Microbiol.* 3:238–250.
2. Brogden, K. A., M. Ackermann, …, B. F. Tack. 2003. Antimicrobial peptides in animals and their role in host defenses. *Int. J. Antimicrob. Agents.* 22:465–478.
3. Hancock, R. E. W., and A. Rozek. 2002. Role of membranes in the activities of antimicrobial cationic peptides. *FEMS Microbiol. Lett.* 206:143–149.
4. Jenssen, H., P. Hamill, and R. E. W. Hancock. 2006. Peptide antimicrobial agents. *Clin. Microbiol. Rev.* 19:491–511.
5. Seelig, J. 2004. Thermodynamics of lipid-peptide interactions. *Biochim. Biophys. Acta.* 1666:40–50.
6. Shai, Y. 1999. Mechanism of the binding, insertion and destabilization of phospholipid bilayer membranes by α-helical antimicrobial and cell non-selective membrane-lytic peptides. *Biochim. Biophys. Acta.* 1462:55–70.
7. White, S. H., and W. C. Wimley. 1999. Membrane protein folding and stability: physical principles. *Annu. Rev. Biophys. Biomol. Struct.* 28:319–365.
8. Zasloff, M. 2002. Antimicrobial peptides of multicellular organisms. *Nature.* 415:389–395.
9. Epand, R. M., and H. J. Vogel. 1999. Diversity of antimicrobial peptides and their mechanisms of action. *Biochim. Biophys. Acta.* 1462:11–28.
10. Ferre, R., M. N. Melo, …, M. Castanho. 2009. Synergistic effects of the membrane actions of cecropin-melittin antimicrobial hybrid peptide BP100. *Biophys. J.* 96:1815–1827.
11. Hancock, R. E. W., and D. S. Chapple. 1999. Peptide antibiotics. *Antimicrob. Agents Chemother.* 43:1317–1323.
12. Huang, H. W. 2000. Action of antimicrobial peptides: two-state model. *Biochemistry.* 39:8347–8352.
13. Huang, H. W. 2006. Molecular mechanism of antimicrobial peptides: the origin of cooperativity. *Biochim. Biophys. Acta.* 1758:1292–1302.
14. Melo, M. N., R. Ferre, and M. A. R. B. Castanho. 2009. Antimicrobial peptides: linking partition, activity and high membrane-bound concentrations. *Nat. Rev. Microbiol.* 7:245–250.
15. Shai, Y. 2002. Mode of action of membrane active antimicrobial peptides. *Biopolymers.* 66:236–248.
16. Tossi, A., L. Sandri, and A. Giangaspero. 2000. Amphipathic, α-helical antimicrobial peptides. *Biopolymers.* 55:4–30.
17. van den Bogaart, G., J. V. Guzmán, …, B. Poolman. 2008. On the mechanism of pore formation by melittin. *J. Biol. Chem.* 283:33854–33857.
18. Yang, L., T. A. Harroun, …, H. W. Huang. 2001. Barrel-stave model or toroidal model? A case study on melittin pores. *Biophys. J.* 81:1475–1485.
19. Huang, H. W., F. Y. Chen, and M. T. Lee. 2004. Molecular mechanism of peptide-induced pores in membranes. *Phys. Rev. Lett.* 92:198304.
20. Ludtke, S. J., K. He, …, H. W. Huang. 1996. Membrane pores induced by magainin. *Biochemistry.* 35:13723–13728.
21. Qian, S., W. Wang, …, H. W. Huang. 2008. Structure of the alamethicin pore reconstructed by x-ray diffraction analysis. *Biophys. J.* 94:3512–3522.
22. Subbalakshmi, C., and N. Sitaram. 1998. Mechanism of antimicrobial action of indolicidin. *FEMS Microbiol. Lett.* 160:91–96.
23. Yeaman, M. R., and N. Y. Yount. 2003. Mechanisms of antimicrobial peptide action and resistance. *Pharmacol. Rev.* 55:27–55.
24. Jean-François, F., J. Elezgaray, …, E. J. Dufourc. 2008. Pore formation induced by an antimicrobial peptide: electrostatic effects. *Biophys. J.* 95:5748–5756.
25. Leontiadou, H., A. E. Mark, and S. J. Marrink. 2006. Antimicrobial peptides in action. *J. Am. Chem. Soc.* 128:12156–12161.
26. Sengupta, D., H. Leontiadou, …, S. J. Marrink. 2008. Toroidal pores formed by antimicrobial peptides show significant disorder. *Biochim. Biophys. Acta.* 1778:2308–2317.
27. Jelokhani-Niaraki, M., R. S. Hodges, …, L. Wheaton. 2008. Interaction of gramicidin S and its aromatic amino-acid analog with phospholipid membranes. *Biophys. J.* 95:3306–3321.
28. Jelokhani-Niaraki, M., E. J. Prenner, …, R. S. Hodges. 2002. Conformation and interaction of the cyclic cationic antimicrobial peptides in lipid bilayers. *J. Pept. Res.* 60:23–36.
29. Matsuzaki, K. 2009. Control of cell selectivity of antimicrobial peptides. *Biochim. Biophys. Acta.* 1788:1687–1692.
30. Gibbs, A. C., L. H. Kondejewski, …, D. S. Wishart. 1998. Unusual β-sheet periodicity in small cyclic peptides. *Nat. Struct. Biol.* 5:284–288.
31. Lee, D. L., and R. S. Hodges. 2003. Structure-activity relationships of de novo designed cyclic antimicrobial peptides based on gramicidin S. *Biopolymers.* 71:28–48.
32. Prenner, E. J., R. N. A. H. Lewis, and R. N. McElhaney. 1999. The interaction of the antimicrobial peptide gramicidin S with lipid bilayer model and biological membranes. *Biochim. Biophys. Acta.* 1462:201–221.
33. Mak, D. O. D., and W. W. Webb. 1995. Two classes of alamethicin transmembrane channels: molecular models from single-channel properties. *Biophys. J.* 69:2323–2336.
34. Mihailescu, D., and J. C. Smith. 1999. Molecular dynamics simulation of the cyclic decapeptide antibiotic, gramicidin S, in dimethy8l sulfoxide solution. *J. Phys. Chem. B.* 103:1586–1594.
35. Mihailescu, D., and J. C. Smith. 2000. Atomic detail peptide-membrane interactions: molecular dynamics simulation of gramicidin S in a DMPC bilayer. *Biophys. J.* 79:1718–1730.

36. Stavrakoudis, A., I. G. Tsoulos, …, T. V. Ovchinnikova. 2009. Molecular dynamics simulation of antimicrobial peptide arenicin-2: β-hairpin stabilization by noncovalent interaction. *Peptide.* 92:143–155.
37. Khalfa, A., and M. Tarek. 2010. On the antibacterial action of cyclic peptides: insights from coarse-grained MD simulations. *J. Phys. Chem. B.* 114:2676–2684.
38. Monroc, S., E. Badosa, …, L. Feliu. 2006. Improvement of cyclic decapeptides against plant pathogenic bacteria using a combinatorial chemistry approach. *Peptides.* 27:2575–2584.
39. Monroc, S., E. Badosa, …, E. Bardají. 2006. De novo designed cyclic cationic peptides as inhibitors of plant pathogenic bacteria. *Peptides.* 27:2567–2574.
40. Case, D. A., T. A. Darden, …, P. A. Kollman, editors. 2006. AMBER 9, University of California at San Francisco, San Francisco, CA.
41. Kabsch, W., and C. Sander. 1983. Dictionary of protein secondary structure: pattern recognition of hydrogen-bonded and geometrical features. *Biopolymers.* 22:2577–2637.
42. Van Der Spoel, D., E. Lindahl, …, H. J. Berendsen. 2005. GROMACS: fast, flexible, and free. *J. Comput. Chem.* 26:1701–1718.
43. van Gunsteren, W. F., P. Krüger, …, I. G. Tironi. 1996. Biomolecular Simulation: The GROMOS96 Manual and User Guide. vdf Hochschulverlag AG an der ETH Zürich and BIOMOS b.v., Zürich, Switzerland.
44. Anézo, C., A. H. de Vries, …, S. J. Marrink. 2003. Methodological issues in lipid bilayer simulations. *J. Phys. Chem. B.* 107:9424–9433.
45. Zhao, W., T. Róg, …, M. Karttunen. 2007. Atomic-scale structure and electrostatics of anionic palmitoyloleoylphosphatidylglycerol lipid bilayers with Na^+ counterions. *Biophys. J.* 92:1114–1124.
46. Pabst, G., S. Danner, …, V. A. Raghunathan. 2007. On the propensity of phosphatidylglycerols to form interdigitated phases. *Biophys. J.* 93:513–525.
47. Tironi, I. G., R. Sperb, …, W. F. van Gunsteren. 1995. A generalized reaction field method for molecular dynamics simulations. *J. Chem. Phys.* 102:5451–5459.
48. Berendsen, H. J. C., J. P. M. Postma, …, J. Hermans. 1981. Interaction models for water in relation to protein hydration. *In* Intermolecular Forces. P. Pullman, editor. Reidel, Dordrecht, The Netherlands. 331–342.
49. Berendsen, H. J. C., J. P. M. Postma, …, J. R. Haak. 1984. Molecular dynamics with coupling to an external bath. *J. Chem. Phys.* 81:3684–3690.
50. Yesylevskyy, S., S. J. Marrink, and A. E. Mark. 2009. Alternative mechanisms for the interaction of the cell-penetrating peptides penetratin and the TAT peptide with lipid bilayers. *Biophys. J.* 97:40–49.
51. Bond, P. J., and S. Khalid. 2010. Antimicrobial and cell-penetrating peptides: structure, assembly and mechanisms of membrane lysis via atomistic and coarse-grained molecular dynamics simulations. *Protein Pept. Lett.* 17:1313–1327.
52. Mátyus, E., C. Kandt, and D. P. Tieleman. 2007. Computer simulation of antimicrobial peptides. *Curr. Med. Chem.* 14:2789–2798.
53. Mueller, P., D. O. Rudin, …, W. C. Wescott. 1962. Reconstitution of cell membrane structure in vitro and its transformation into an excitable system. *Nature.* 194:979–980.
54. Mueller, P., D. O. Rudin, …, W. C. Wescott. 1962. Reconstitution of excitable cell membrane structure in vitro. *Circulation.* 26:1167–1171.
55. Mueller, P., D. O. Rudin, …, W. C. Wescott. 1963. Methods for the formation of single biomolecular lipid membranes in aqueous solution. *J. Phys. Chem.* 67:534–535.
56. Salay, L. C., J. Procopio, …, S. Schreier. 2004. Ion channel-like activity of the antimicrobial peptide Tritrpticin in planar lipid bilayers. *FEBS Lett.* 565:171–175.
57. Hille, B. 1968. Pharmacological modifications of the sodium channels of frog nerve. *J. Gen. Physiol.* 51:199–219.
58. Hille, B. 2001. Ionic Channels of Excitable Membranes. Sinauer, Sunderland, MA.
59. Cruickshank, C. C., R. F. Minchin, …, B. Martinac. 1997. Estimation of the pore size of the large-conductance mechanosensitive ion channel of *Escherichia coli*. *Biophys. J.* 73:1925–1931.
60. van den Bogaart, G., V. Krasnikov, and B. Poolman. 2007. Dual-color fluorescence-burst analysis to probe protein efflux through the mechanosensitive channel MscL. *Biophys. J.* 92:1233–1240.
61. van den Bogaart, G., J. T. Mika, …, B. Poolman. 2007. The lipid dependence of melittin action investigated by dual-color fluorescence burst analysis. *Biophys. J.* 93:154–163.
62. Doeven, M. K., J. H. Folgering, …, B. Poolman. 2005. Distribution, lateral mobility and function of membrane proteins incorporated into giant unilamellar vesicles. *Biophys. J.* 88:1134–1142.
63. van den Bogaart, G., I. Kusters, …, B. Poolman. 2008. Dual-color fluorescence-burst analysis to study pore formation and protein-protein interactions. *Methods.* 46:123–130.
64. Mika, J. T., G. Moiset, …, B. Poolman. 2011. Structural basis for the enhanced activity of cyclic antimicrobial peptides: the case of BPC194. *Biochim. Biophys. Acta.*, In press.
65. Gregory, S. M., A. Cavenaugh, …, P. F. Almeida. 2008. A quantitative model for the all-or-none permeabilization of phospholipid vesicles by the antimicrobial peptide cecropin A. *Biophys. J.* 94:1667–1680.
66. Rzepiela, A. J., D. Sengupta, …, S. J. Marrink. 2010. Membrane poration by antimicrobial peptides combining atomistic and coarse-grained descriptions. *Faraday Discuss.* 144:431–443.
67. Colombo, G., F. Curnis, …, A. Corti. 2002. Structure-activity relationships of linear and cyclic peptides containing the NGR tumor-homing motif. *J. Biol. Chem.* 277:47891–47897.
68. Ashrafuzzaman, M., O. S. Andersen, and R. N. McElhaney. 2008. The antimicrobial peptide gramicidin S permeabilizes phospholipid bilayer membranes without forming discrete ion channels. *Biochim. Biophys. Acta.* 1778:2814–2822.
69. Duclohier, H., G. Molle, and G. Spach. 1989. Antimicrobial peptide magainin I from *Xenopus* skin forms anion-permeable channels in planar lipid bilayers. *Biophys. J.* 56:1017–1021.